ELSEVIER

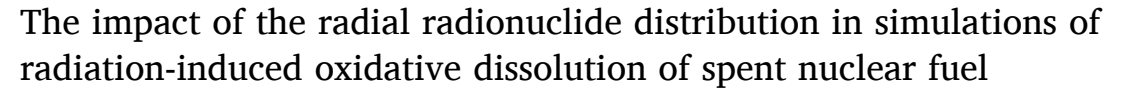
Contents lists available at ScienceDirect

Nuclear Engineering and Technology

journal homepage: www.elsevier.com/locate/net



Original Article





- ^a Swedish Nuclear Fuel and Waste Management Co., SE-101 24, Stockholm, Sweden
- b School of Engineering Sciences in Chemistry, Biotechnology and Health, Department of Chemistry, KTH Royal Institute of Technology, SE-100 44, Stockholm, Sweden

ARTICLE INFO

Keywords: Spent nuclear fuel Radionuclide inventory Rim-effect Radiolysis Dose rate

ABSTRACT

One of the key-features in the safety assessment of geological repositories for spent nuclear fuel is the rate of radionuclide release from fuel in contact with groundwater. This process is driven by the radioactivity of the fuel itself through the radiolysis of the groundwater producing oxidative species capable of converting the fuel matrix (UO₂) to more soluble U(VI). Models describing this process are often based on the spatial dose rate distribution which is derived from the radionuclide inventory (often considered to be homogeneously distributed in the fuel). However, in reality the inventory is radially distributed with higher concentrations of fission- and neutron activation products closer to the fuel pellet surface. In this work, we have explored the impact of the spatial radionuclide distribution on the dose rate profile and rate of fuel matrix dissolution using SCALE and MCNP calculations in combination with a previously developed steady-state approach for radiation-induced dissolution of UO₂. When accounting for the spatial radionuclide distribution, the calculated maximum rate of dissolution is 2–3 times higher than when assuming homogeneous radionuclide distribution.

1. Introduction

The fate of the highly radiotoxic spent nuclear fuel is one of the major challenges for countries utilizing nuclear power. While reprocessing of the spent nuclear fuel to recover the fissile and fertile constituents is often discussed as a means to achieve a more sustainable nuclear fuel cycle, most countries plan to place their spent nuclear fuel in geological repositories where the radiotoxic material will remain isolated from the biosphere until the level of radioactivity has declined to that of a natural uranium ore [1]. In other words, the integrity of the repository must be maintained for at least 100 000 years [1]. The extremely long time period over which the natural and engineered barriers of the repository must persist calls for very thorough safety assessments prior to the construction of such a repository. One of the key-processes that must be accounted for in such safety assessment is the dissolution of spent nuclear fuel in contact with groundwater and the subsequent release of radionuclides [1]. The majority of commercial nuclear fuels used today are based on uranium dioxide (UO2). After use in a nuclear reactor, a small fraction of the uranium has been converted to fission products and heavier actinides [1]. Hence, the main constituent is still UO2. When in contact with groundwater, the release of radionuclides can roughly be divided in two parts. At first, readily soluble radionuclides present at the fuel pellet surface or grain boundaries (the so called "Instant Release Fraction") are released to the groundwater [2]. This process is followed by a considerably slower process where radionuclides are released as a consequence of UO₂-matrix dissolution (containing the major part of the radionuclide inventory) [3]. In general, UO₂ has very low solubility in the anoxic or slightly reducing groundwaters expected to be found at most potential repository sites [4]. However, the inherent radioactivity of the fuel induces radiolysis of water and thereby alters the redox conditions at the interface between the fuel pellet surface and the intruding groundwater. The oxidizing aqueous radiolysis products (HO[•], H₂O₂, HO₂ and O₂) are capable of oxidizing UO₂ to considerably more soluble U(VI) and thereby induce oxidative dissolution of the fuel [3]. Radiation induced oxidative dissolution of UO₂ has been extensively studied since the 1980's and the level of mechanistic understanding must now be considered to be fairly good [1,5,6]. It has been demonstrated that the process is mainly driven by H2O2 [7]. As for any other system where reactive species are formed at a constant rate, the concentration of the reactive species will increase until the rate of consumption balances the rate of production. At this point, steady-state has been reached. Previous studies on radiation induced dissolution of spent

E-mail address: matsj@kth.se (M. Jonsson).

https://doi.org/10.1016/j.net.2025.103814

^{*} Corresponding author.

nuclear fuel have shown that steady-state conditions are expected to be reached within a relatively short time [8,9]. As a consequence, the maximum rate of radiation induced oxidative dissolution of UO $_2$ (under the assumption that H_2O_2 is not consumed in any competing reactions) can be estimated from the rate of H_2O_2 production in the system [10]. In addition, in scenarios of relevance for the safety assessment, radiolysis at the fuel surface is dominated by α radiation [3]. These findings simplify numerical simulations of fuel dissolution considerably [11]. There is also significant evidence that molecular hydrogen formed in water radiolysis and upon anaerobic corrosion of iron (canister material) efficiently inhibit the oxidative dissolution of UO $_2$ [12–15].

The production of H₂O₂ is directly dependent on the geometrical dose rate distribution, i.e., the dose rate as a function of radial distance from the fuel pellet surface, and the amount of available groundwater. In previous work, the geometrical dose rate distributions have been calculated from general specific α activities or from more complete radionuclide inventories of the spent nuclear fuel obtained from calculations [16-22]. In all cases of spent nuclear fuel dissolution modelling known to the authors, the radionuclide inventory has been assumed to be homogeneously distributed in the fuel. However, it is well-known that the radionuclide distribution in irradiated nuclear fuel is not homogeneous [23]. One reason for inhomogeneity in the radionuclide distribution is the locally increased burn-up (and increased concentration of fission products and actinides) in the pellet periphery (rim) caused by less resonance self-shielding. This zone is generally (at BU > 40 MWd/kgU) characterized by a porous and fine-grained microstructure giving a somewhat lower density ($\sim 15 \%$ at 50 MWd/kgU) [23]. It has been discussed whether the radionuclide inventory in the rim should be included in the Instant Release Fraction or if it should be considered part of the matrix inventory [24-26]

As α -radiolysis is the general driving force for the fuel dissolution and α -particles have very short penetration depth in UO₂, the radial distribution of α -emitting radionuclides is expected to have a significant impact on the geometrical dose distribution and thereby also on the rate of spent nuclear fuel dissolution [23]. The α -dose rate profile in water adjacent to the fuel is attributed to α -emitting nuclides in the outermost part of the fuel pellet. If the rim-effect (i.e., the effect of a higher radionuclide inventory in the pellet rim compared to the bulk) mentioned above is accounted for, significantly higher dose rates and thereby also maximum UO2 dissolution rates can be expected compared to the case where a homogeneous distribution of the inventory is assumed. In this work we explore the impact of the radial radionuclide distribution on the geometrical dose rate distribution and the rate of H₂O₂ production in water surrounding a spent fuel pellet. The spent fuel pellet is here represented by a simplified system consisting of a homogeneous UO2 pellet including a radionuclide content, corresponding to that of a spent fuel pellet, distributed between two zones (rim and bulk). The results are discussed in view of maximum UO2 dissolution rates.

2. Methods

The calculations were performed in three steps described in detail below. At first the radial radionuclide inventory was determined and based on this data the effective rim size was chosen; secondly the source strength was determined in different fuel regions and finally dose rate profiles in water surrounding the pellet were calculated based in these source strengths.

2.1. Radial radionuclide inventory and rim size

In this first step the radionuclide distribution was investigated by determining the radionuclide inventory in a 1 μm thick layer at different distances from the pellet surface. The inventory was determined at different pellet radii using the SCALE 6.2.3 2D TRITON depletion sequence (T-DEPL) with the 252-group ENDF/B-VII.I cross section library [27]. An infinite lattice of PWR fuel pins was modelled with a fuel

burnup at 60 MWd/kgU (4.82 % enrichment). A density of 10.45 g/cm³ was assumed in the entire pellet. As mentioned previously, the density is in fact somewhat lower in the outer part of the pellet. A lower density gives a lower source strength although this effect is counteracted by lower radiation shielding. Calculations show that the overall impact of the reduced density in the outer part of the pellet is very marginal. A reduced density by 10 % leads to a reduction in average dose rate by 1 %. We therefore neglect this effect in our further calculations.

2.2. Source strength

Based on the calculated inventory, a rim size of 10^{-5} m (10 μ m) was chosen (see Results and discussion). The source strength in a 10^{-5} m rim was determined using results from TRITON-simulations together with the ORIGEN decay solver within SCALE [27]. α , β and γ particle spectra corresponding to three different burnups were determined, 60 MWd/kgU (4.82 % enrichment), 45 MWd/kgU (3.9 % enrichment) and 30 MWd/kgU (2.95 % enrichment). The source strength after 15 y, 1000 y and 100 000 y of decay was determined for each burnup case and can be found in supplementary information.

Two different fuel regions were used for determining the α source, one region for the outer 10^{-5} m rim and another region for the rest (bulk). The source strength for a homogeneous distribution over the entire cylinder was also determined for all three particle types; $\alpha,\,\beta$ and $\gamma.$

2.3. Dose model geometry

MCNP 6.2 [28] was used to model the absorbed dose in water surrounding a cylindrical pellet of UO₂ ($\rho=10.45~g/cm^3$) with a radius of 4 x 10^{-3} m and a height of 10^{-2} m. A schematic overview of the system is shown in Fig. 1. The source strength is distributed between the bulk and the rim as described above.

The energy deposition, or absorbed dose, at different distances from the uranium pellet lateral surface was determined using a cylindrical superimposed mesh tally (TMESH) of type 3.

2.4. Dose rate from α -radiation

The mesh resolution in MCNP should be small enough to catch the distance dependent dose for α -radiation, but large enough for the assumption of local energy deposition at collision to be valid. Hence,

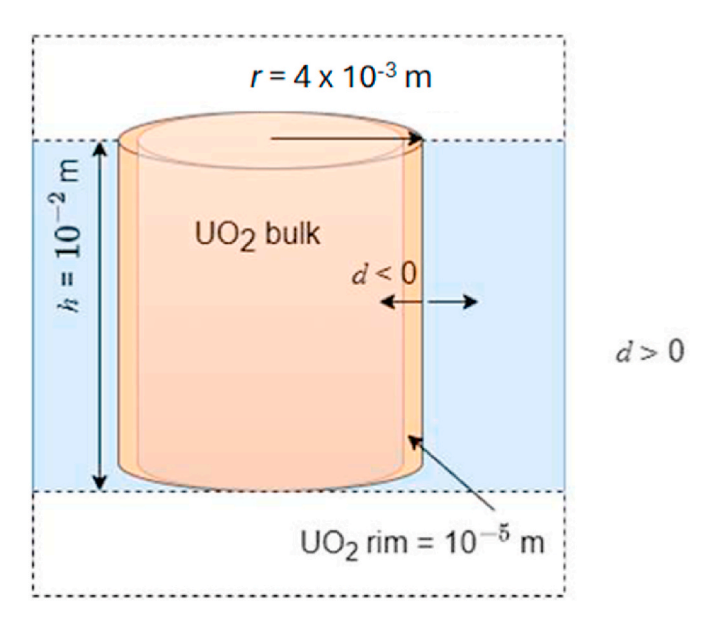


Fig. 1. Schematic overview of the geometry used in the MCNP simulations.

possible secondary particles should have a short range compared to the mesh resolution. A knock-on electron (delta-ray) from a head-on α collision with an α energy, E_{α} , of 5.5 MeV (average energy of α particles at 60 MWd/kgU and 15 y of decay) has the maximum energy of 3 keV (conservation of energy and momentum $E_e = 4 \frac{E_a}{m_e} m_e = 3$ keV, where m_a is the α particle mass and m_e is the electron mass). A 3 keV electron has a range of approximately 2 x 10⁻⁷ m in water, but electrons with maximum energy are rarely produced. The mesh resolution in MCNP was therefore set to 2 x 10^{-7} m in the radial direction. α transport for determining dose rate in MCNP is done using physics models [29]. For energies below 1.31 MeV a continuous slowing down approximation (CSDA) is used based on Lindhard's theory where the material of which the α particles interact with, is assumed to consist of a gas of free electrons [29]. The α particles are assumed to be point charges experiencing Coulomb repulsion from the electron gas. For energies above 5.24 MeV a CSDA-model based on Bethe's theory is used where interaction is taking place by inelastic scattering on bound electrons. Between 1.31 MeV and 5.24 MeV, an interpolation between values calculated using the two models is used. The default cut off for when transport of α particles is terminated and the energy is assumed to be deposited locally is 4 MeV. The minimum value for cut off, 1 keV was used instead. The number of simulated particles was 2 x 10⁶.

The dose rate in water was determined for two different source distributions. In the first case a homogeneous average distribution of the source in the entire pellet volume was assumed. In the second case one MCNP simulation was made with source only at the $10^{-5}\, m$ rim section and an additional MCNP simulation was made with the source particles in the bulk section, until $10^{-5}\, m$ from the side surface of the pellet cylinder. The dose rate including rim effect was then determined by adding the results from the simulations with the source at the rim and the source in the bulk. α particles of 5.5 MeV have a range of about 4 x $10^{-5}\, m$ in water [30] and the average dose rate from α radiation was determined over this distance for each case.

Both the γ - and β -radiation typically have ranges much longer than $10^{-5}\,$ m in UO2, which means that a larger rim would have to be considered in these cases. However, a larger rim also weakens the effect and studies of possible rim effects for β particles (nor γ) is not included in this study.

2.5. β -radiation

The mesh resolution was set to 2 x 10^{-6} m in the radial direction. Both electrons and secondary photons were transported (MODE E P) and the number of source particles was 1 x 10^7 . The average energy of a source β -particle, according to SCALE simulations at 60 MWd/kgU and 15 y of decay, is around 300 keV, with a range of 8 x 10^{-3} m in water and 2 x 10^{-4} m in uranium oxide [30]. Hence, a rim size of 10^{-5} m is too small for β -radiation and simulations in MCNP was done only for a homogeneous source distribution. The average dose was determined over 4 x 10^{-5} m and 10^{-2} m in water.

2.6. γ -radiation

The mesh resolution was set to 5 x 10^{-6} m in the radial direction. Both electrons and secondary photons were transported (MODE E P) and the number of source particles was 1 x 10^7 . The dose was determined at distances up to 0.1 m from the fuel pellet, which is a reasonable maximum distance to the fuel canister. The height of the MCNP model was merely 10^{-2} m and reflective boundary surfaces at top and bottom where therefore used in the γ transport simulations in order to avoid underestimated dose rates. Simulations in MCNP was done only for a homogeneous source distribution and the average dose was determined over 4 x 10^{-5} m, 10^{-2} m and 0.1 m in water.

2.7. Laser Ablation Inductively Coupled Plasma Mass Spectrometry (LA-ICP-MS)

The results from the modelling of the radial radionuclide distribution has been compared to radionuclide profiles measured by Laser Ablation Inductively Coupled Plasma Mass Spectrometry (LA-ICP-MS). The LA-ICP-MS analysis was performed at the Hot Cell Laboratory of Studsvik Nuclear AB within the Collaborative Project "Fast/Instant Release of Safety Relevant Radionuclides from Spent Nuclear Fuel" (7th EC FP CP FIRST-Nuclides). Further description of the method can be found in Refs. [31,32]. The fuel sample used was cut from a BWR rod irradiated with burn-up (rod average) 57.1 MWd/kgU. The ablation equipment consists of a New-Wave UP-213 Nd:YAG laser connected to an ablation chamber that is housed in a hot cell. A carrier gas (Ar, He or <1 % H2 in He) transports the created aerosol for analysis to an Inductively Coupled Plasma Mass Spectrometer (ICP-MS) installed in a glove box. In this study a 20 Hz ablation frequency, spot size between 6×10^{-5} m and line speed of $1-3 \times 10^{-5}$ m/s was used. Further information about the fuel and experimental details can be found in Ref. [31], where also some of the radial profiles obtained in the study were published.

3. Results and discussion

In order to determine the rim size, the radionuclide inventory was determined at different pellet radii using SCALE as described above. The resulting inventory profiles were compared to experimental data obtained by LA-ICP-MS. Examples for 133 Cs and 239 Pu are shown in Figs. 2 and 3.

In the figures the LA-ICP-MS results are plotted as fraction of ²³⁸U. It should however be noted that, due to the lack of suitable reference materials, the units should be regarded as arbitrary and an exact match with the mass fraction obtained by the SCALE calculations is not expected. In Figs. 2 and 3 it is shown that the SCALE calculations reproduce the radionuclide distribution of ²³⁹Pu and ¹³³Cs quite well. The relative distribution of ²³⁹Pu between the bulk and the rim is very well reproduced. For ¹³³Cs (Fig. 2) it can be noted that the increase close to the pellet surface as measured by LA-ICP-MS is much sharper compared to the increase calculated by SCALE. This can be attributed to relocation of Cs during operating temperatures, which can also be noted as ¹³³Cs peaks attributed to cracks in the fuel.

From these results it can be concluded that the most pronounced increase in the radionuclide inventory is observed in the outermost 2 x $10^{-4}\,\text{m}$ of the fuel pellet. However, α particles from the region $>\!10^{-5}\,\text{m}$ from the fuel surface lose most of their energy in the UO $_2$ matrix and are not expected to contribute significantly to the dose rate in the surrounding water. This was verified by modelling the dose rate contribution from the region $1\!-\!2$ x $10^{-5}\,\text{m}$ from the fuel surface in a 15-year-old fuel with 60 Mwd/kgU burn-up (4.82 % enrichment). The results show that this region contributes with less than 1 % to the average dose rate in 4 x $10^{-5}\,\text{m}$ water. Based on these results, a rim size of $10^{-5}\,\text{m}$ was chosen when modelling the dose rate in the present work.

The difference in inventory between the bulk and rim depends somewhat on the radionuclide. For ^{239}Pu , which is one of the main contributors to the α dose, the specific inventory as determined by SCALE calculations at 60 MWd/kgU is a factor of four higher at the outermost 10^{-6} m layer compared to the pellet-centre inventory and a factor of three higher compared to the average pellet inventory. The specific inventory of ^{239}Pu in the outer 10^{-5} m layer is only 10 % less than the inventory in the outer 10^{-6} m layer, which means that 10^{-5} m is thin enough for determining the α inventory at the surface.

Using a rim size of 10^{-5} m, two different fuel regions were used for determining the α source, one region for the outer 10^{-5} m rim and another region for the rest. The source strength for a homogeneous distribution over the entire cylinder was also determined for all three radiation types, α , β and γ . Resulting source strengths are presented in Table 1.

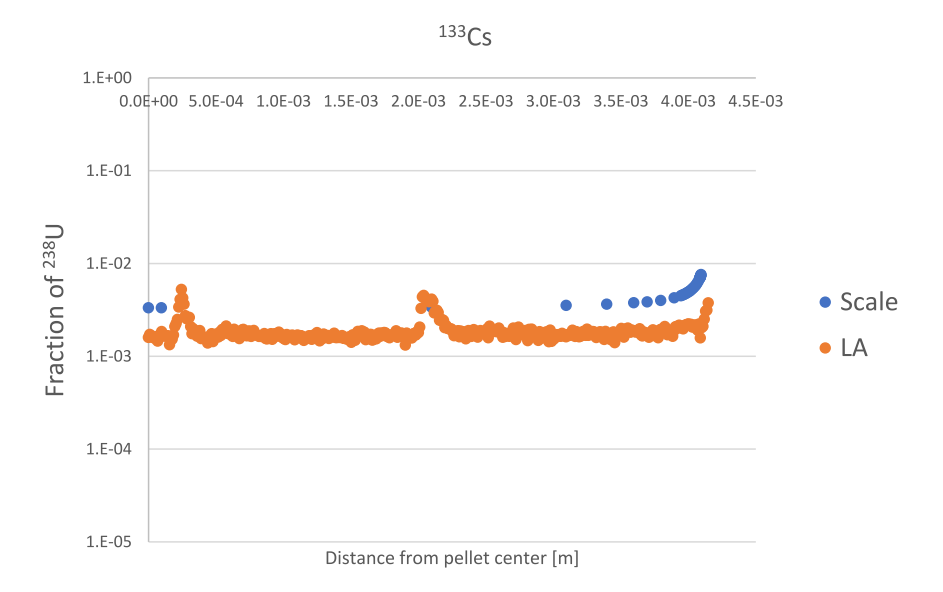


Fig. 2. Radial distribution of ¹³³Cs determined by SCALE calculations and by LA-ICP-MS.



Fig. 3. Radial distribution of ²³⁹Pu determined by SCALE calculations and by LA-ICP-MS.

Based on the source strengths presented in Table 1, the geometrical dose rate profiles were calculated using MCNP. In Fig. 4, the $\alpha\text{-}dose$ rate profiles for fuel with burnup 60 MWd/kgU and age 15 y are plotted for a homogeneous radionuclide inventory and for the case where the rimeffect is accounted for.

As can be seen, the dose rate profiles differ significantly and it is clear that more energy is deposited in the aqueous phase when the actual radial radionuclide inventory distribution is accounted for. As it has previously been shown that the production rate of $\rm H_2O_2$ attributed to α -radiolysis can be calculated from the average dose rate within the irradiated volume (i.e., the actual profile does not need to be accounted for) [5], we have calculated the average dose rates for all cases included in this study.

In Table 2 a-c, the calculated average dose rates attributed to α -, β - and γ -radiation, respectively, at three different burnups (30, 45 and 60 MWd/kgU) and three different fuel ages (15, 1000 and 100 000 years)

are given. More detailed information on dose rates as function of the distance from interface for the 60 MWd/kgU case can be found in supplementary information. For α -radiation both the dose rate based on homogeneous radionuclide distribution and the dose rate based on the rim-effect are given. The dose rates are averaged over the water volume limited by the distance from the fuel surface. In the tables below, 4 x $10^{-5}\,\text{m}$, $10^{-2}\,\text{m}$ and 0.1 m are used. It should be noted that the dose rate referred to as α : Rim is calculated from the rim inventory for the outer $10^{-5}\,\text{m}$ in combination with the homogeneous inventory for the inner part of the pellet.

As can be seen in Table 2 a, accurately accounting for the radial radionuclide distribution has a significant impact on the average $\alpha\text{-}dose$ rate. In general, the average $\alpha\text{-}dose$ rate within the 4 x 10^{-5} m limiting the penetration depth of $\alpha\text{-}particles$ in water is 2–3 times higher when accounting for the rim effect. This is a significant difference that cannot be neglected. As can also be seen, the contribution from $\beta\text{-}$ and

 Table 1

 Source strength in per second and gram of heavy metal (uranium) for different burnups and decay times.

Fuel age		Source strength (s ⁻¹ g _{HM})		
		60 MWd/kgU	45 MWd/kgU	30 MWd/kgU
15 y	α: Homogeneous	8.52 x 10 ⁸	5.16 x 10 ⁸	2.62 x 10 ⁸
	α: Rim	1.72 x 10 ⁹	1.07 x 10 ⁹	5.01 x 10 ⁸
	β: Homogeneous	1.64 x 10 ¹⁰	1.27 x 10 ¹⁰	8.89 x 10 ⁹
	γ: Homogeneous	9.06 x 10 ⁹	6.78 x 10 ⁹	4.53 x 10 ⁹
1000 y	α: Homogeneous	1.13 x 10 ⁸	9.44 x 10 ⁷	7.25 x 10 ⁷
	α: Rim	3.38 x 10 ⁸	2.82 x 10 ⁸	1.99 x 10 ⁸
	β: Homogeneous	3.29 x 10 ⁶	2.18 x 10 ⁶	1.19 x 10 ⁶
	γ: Homogeneous	5.15 x 10 ⁷	4.10 x 10 ⁷	2.98 x 10 ⁷
100 000 у	α: Homogeneous	2.23 x 10 ⁶	1.78 x 10 ⁶	1.35 x 10 ⁶
	α: Rim	5.17 x 10 ⁶	4.33 x 10 ⁶	3.29 x 10 ⁶
	β: Homogeneous	1.33 x 10 ⁶	1.00 x 10 ⁶	6.77 x 10 ⁵
	γ: Homogeneous	8.28 x 10 ⁵	6.14 x 10 ⁵	4.13 x 10 ⁵

 $\gamma\text{-radiation}$ within 4 x 10^{-5} m is only significant for the youngest fuel (15 y).

In the event that the accessible water volume exceeds the penetration depth of α -particles, the relative impact of β - and γ -radiation may increase. To assess this, we have calculated the corresponding rate of H₂O₂ production under the different conditions represented in Table 2. The H₂O₂ production rate is calculated from the average dose rate and the radiation chemical yield (G-value) for H2O2 for the respective type of radiation [33]. By accounting for the maximum distance from the fuel surface over which the dose rate is averaged, the H₂O₂ production rate is expressed in mol m⁻² s⁻¹. The H_2O_2 production rate corresponds to the maximum rate of oxidative dissolution of the UO₂-matrix [8-10]. It is well-known that H₂O₂ undergoes catalytic decomposition on oxide surfaces and that solutes present in groundwater may display reactivity towards H₂O₂ [34]. The presence of rare earth metal oxides (fission products) in the UO2-matrix increases the fraction of H2O2 that undergoes catalytic decomposition considerably. Also, β - and γ -radiolysis will contribute to the consumption of H_2O_2 formed by α -radiolysis. Hence, there are a number of processes competing with the oxidation of the UO₂ surface. Furthermore, while the H₂O₂ production rate due to α-radiolysis can be determined quite accurately in the way described above, the same approach will result in significant overestimations for β and γ-radiolysis. Keeping this in mind, we can allow ourselves to compare the impact of α -, β - and γ -radiation in the cases described in Table 2 a-c. The calculated H₂O₂ production rates are given in Table 3 a-c.

Table 2 a Average dose rates over 4×10^{-5} m for fuels of different burn-ups and age.

Fuel age		Dose rate (Gy h ⁻¹)		
		60 MWd/kgU	45 MWd/kgU	30 MWd/kgU
15 y	α: Homogeneous	1100	655	324
	α: Rim	2150	1300	589
	β: Homogeneous	1030	773	530
	γ: Homogeneous	238	181	119
1000 y	α: Homogeneous	127	105	80.7
	α: Rim	375	313	219
	β: Homogeneous	6.32×10^{-2}	4.21×10^{-2}	2.32×10^{-2}
	γ: Homogeneous	8.48×10^{-2}	6.16×10^{-2}	3.73×10^{-2}
100 000 y	α: Homogeneous	2.57	2.04	1.52
	α: Rim	5.69	4.72	3.53
	β: Homogeneous	4.47×10^{-2}	3.22×10^{-2}	2.16×10^{-2}
	γ: Homogeneous	1.42×10^{-2}	9.92×10^{-3}	6.16×10^{-3}

Table 2 b Average dose rates over 10^{-2} m for fuels of different burn-ups and age.

Fuel age		Dose rate (Gy h ⁻¹)		
		60 MWd/kgU	45 MWd/kgU	30 MWd/kgU
15 y	β: Homogeneous γ: Homogeneous	85.1 60.9	64.6 45.2	44.0 29.9
1000 у	β: Homogeneous γ: Homogeneous	1.25 x 10 ⁻³ 3.95 x 10 ⁻³	9.17×10^{-4} 2.78×10^{-3}	5.94 x 10 ⁻⁴ 1.70 x 10 ⁻³
100 000 y	β: Homogeneous γ: Homogeneous	2.48×10^{-3} 3.53×10^{-3}	$ \begin{array}{c} 1.80 \times 10^{-3} \\ 2.45 \times 10^{-3} \end{array} $	1.20×10^{-3} 1.51×10^{-3}

Table 2 c
Average dose rate over 0.1 m for fuels of different burn-ups and age.

Fuel age		Dose rate (Gy h ⁻¹)		
		60 MWd/kgU	45 MWd/kgU	30 MWd/kgU
15 y 1000 y 100 000 y	γ: Homogeneous γ: Homogeneous γ: Homogeneous	13.4 8.31 x 10 ⁻⁴ 7.94 x 10 ⁻⁴	9.94 5.83 x 10 ⁻⁴ 5.51 x 10 ⁻⁴	6.56 3.51 x 10 ⁻⁴ 3.40 x 10 ⁻⁴

As already mentioned in connection to the average dose rates, the rim-effect is significant. Depending on the accessible water volume, as reflected by the distance from the fuel surface, and the fuel age, we can draw some interesting conclusions regarding the relative contribution from the different types of radiation. Starting with the $4\times10^{-5}\,m$ case, it

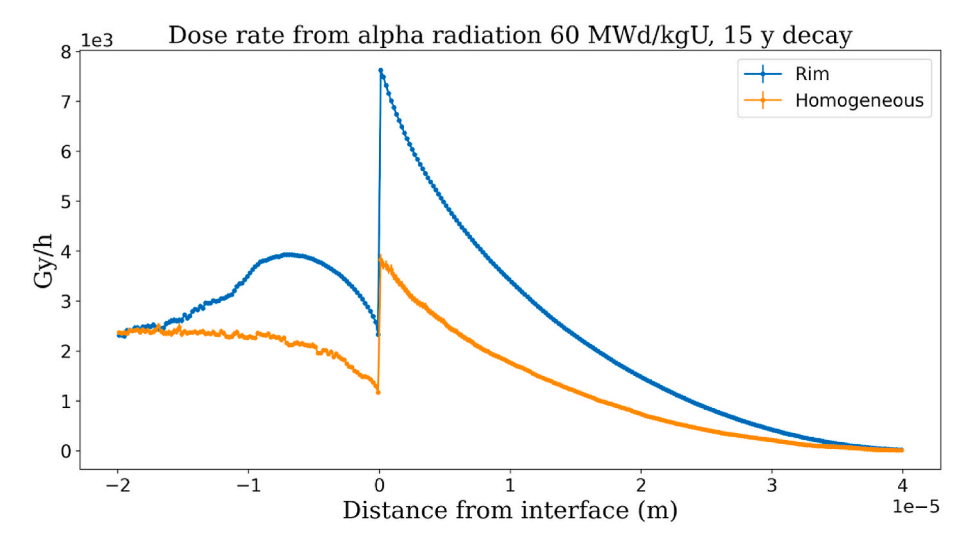


Fig. 4. α -dose rate profiles for fuel with burnup 60 MWd/kgU, age 15 y for a homogeneous radionuclide inventory and for the case where the rim-effect is accounted for.

Table 3 a H_2O_2 production rate attributed to $\alpha\text{-},~\beta\text{-}$ and $\gamma\text{-radiolysis}$ over 4 x 10^{-5} m for fuels of different burn-up and age.

Fuel age		$\rm H_2O_2$ production rate (mol m ⁻² s ⁻¹)		
		60 MWd/ kgU	45 MWd/ kgU	30 MWd/ kgU
15 y	α: Homogeneous α: Rim β: Homogeneous γ: Homogeneous Total ^a : Homogeneous Total ^b : Rim	1.22 x 10 ⁻⁹ 2.39 x 10 ⁻⁹ 8.01 x 10 ⁻¹⁰ 1.85 x 10 ⁻¹⁰ 2.21 x 10 ⁻⁹ 3.38 x 10 ⁻⁹	7.28 x 10^{-10} 1.44 x 10^{-9} 6.01 x 10^{-10} 1.41 x 10^{-10} 1.47 x 10^{-9} 2.19 x 10^{-9}	3.60 x 10 ⁻¹⁰ 6.54 x 10 ⁻¹⁰ 4.12 x 10 ⁻¹⁰ 9.26 x 10 ⁻¹¹ 8.65 x 10 ⁻¹⁰
1000 y	α: Homogeneous α: Rim β: Homogeneous γ: Homogeneous Total ^a : Homogeneous Total ^b : Rim	$ \begin{array}{c} 1.41 \times 10^{-10} \\ 4.17 \times 10^{-10} \\ 4.92 \times 10^{-14} \\ 6.60 \times 10^{-14} \\ 1.41 \times 10^{-10} \end{array} $ $ 4.17 \times 10^{-10} $	$ \begin{array}{c} 1.17 \times 10^{-10} \\ 3.48 \times 10^{-10} \\ 3.27 \times 10^{-14} \\ 4.79 \times 10^{-14} \\ 1.17 \times 10^{-10} \end{array} $ 3.48×10^{-10}	8.97 x 10 ⁻¹¹ 2.43 x 10 ⁻¹⁰ 1.80 x 10 ⁻¹⁴ 2.90 x 10 ⁻¹⁴ 8.97 x 10 ⁻¹¹
100 000 y	α: Homogeneous α: Rim β: Homogeneous γ: Homogeneous Total ^a : Homogeneous Total ^b : Rim	2.86×10^{-12} 6.32×10^{-12} 3.48×10^{-14} 1.10×10^{-14} 2.90×10^{-12} 6.37×10^{-12}	2.27×10^{-12} 5.24×10^{-12} 2.50×10^{-14} 7.72×10^{-15} 2.30×10^{-12} 5.28×10^{-12}	1.69 x 10 ⁻¹² 3.92 x 10 ⁻¹² 1.68 x 10 ⁻¹⁴ 4.79 x 10 ⁻¹⁵ 1.71 x 10 ⁻¹² 3.94 x 10 ⁻¹²

 $[^]a$ The sum of contributions from α (homogeneous), β and γ within 4 x 10^{-5} m from the surface.

Table 3 b H_2O_2 production rate attributed to $\beta\text{-}$ and $\gamma\text{-}radiolysis$ over 10^{-2} m for fuels of different burn-up and age.

Fuel age		${\rm H_2O_2}$ production rate (mol m $^{-2}$ s $^{-1}$)		
		60 MWd/ kgU	45 MWd/ kgU	30 MWd/ kgU
15 y	β: Homogeneous γ: Homogeneous Total ^a : Homogeneous Total ^b : Rim	1.65×10^{-8} 1.18×10^{-8} 2.96×10^{-8} 3.08×10^{-8}	1.26 x 10 ⁻⁸ 8.79 x 10 ⁻⁹ 2.21 x 10 ⁻⁸ 2.28 x 10 ⁻⁸	8.56 x 10 ⁻⁹ 5.81 x 10 ⁻⁹ 1.47 x 10 ⁻⁸ 1.50 x 10 ⁻⁸
1000 y	β: Homogeneous γ: Homogeneous Total ^a : Homogeneous Total ^b : Rim	2.43×10^{-13} 7.68×10^{-13} 1.42×10^{-10} 4.18×10^{-10}	1.78 x 10 ⁻¹³ 5.41 x 10 ⁻¹³ 1.17 x 10 ⁻¹⁰ 3.48 x 10 ⁻¹⁰	$ \begin{array}{c} 1.16 \times 10^{-13} \\ 3.31 \times 10^{-13} \\ 9.01 \times 10^{-11} \end{array} $ 2.44 x 10 ⁻¹⁰
100 000 y	β: Homogeneous γ: Homogeneous Total ^a : Homogeneous Total ^b : Rim	4.82 x 10 ⁻¹³ 6.86 x 10 ⁻¹³ 4.02 x 10 ⁻¹² 7.49 x 10 ⁻¹²	3.50×10^{-13} 4.76×10^{-13} 3.09×10^{-12} 6.07×10^{-12}	2.33×10^{-13} 2.94×10^{-13} 2.22×10^{-12} 4.45×10^{-12}

^a The sum of contributions from α (homogeneous) within 4 x 10⁻⁵ m from the surface (Table 3 a) and β and γ within 10⁻² m from the surface.

is evident that the contribution from α -radiation varies between 40 and 70 % for the youngest fuel age (15 y). The higher values correspond to the cases where the rim-effect is accounted for. For fuel ages 1000 and 100 000 y, the contribution from α -radiation corresponds to 98–100 %. For the 10^{-2} m case, the relative contribution from α -radiation is 5–10 % for the youngest fuel age, 100 % for fuel age 1000 y and 70–85 % for fuel age 100 000 y. The higher values for the youngest and the oldest fuel correspond to cases where the rim-effect is accounted for. For the 0.1 m case, the relative contribution from α -radiation is 2–5.3 % for the youngest fuel age, close to 100 % for fuel age 1000 y and ca. 60–80 % at

Table 3 c ${\rm H_{2}O_{2}}$ production rate attributed to γ -radiolysis over 0.1 m for fuels of different burn-up and age.

Fuel age		$\rm H_2O_2$ production rate (mol m ⁻² s ⁻¹)		
		60 MWd/ kgU	45 MWd/ kgU	30 MWd/ kgU
15 y	γ: Homogeneous Total ^a : Homogeneous	2.61×10^{-8} 4.38×10^{-8}	1.93 x 10 ⁻⁸ 3.26 x 10 ⁻⁸	1.28 x 10 ⁻⁸ 2.17 x 10 ⁻⁸
	Total ^b : Rim	4.50×10^{-8}	3.33×10^{-8}	2.20×10^{-8}
1000 у	γ: Homogeneous Total ^a :	1.62×10^{-12} 1.43×10^{-10}	$ \begin{array}{c} 1.13 \times 10^{-12} \\ 1.18 \times 10^{-10} \end{array} $	6.83 x 10 ⁻¹³ 9.05 x 10 ⁻¹¹
	Homogeneous Total ^b : Rim	4.19 x 10 ⁻¹⁰	3.49×10^{-10}	2.44 x 10 ⁻¹⁰
100 000	γ: Homogeneous	1.54 x 10 ⁻¹²	1.07 x 10 ⁻¹²	6.61 x 10 ⁻¹³
у	Total ^a : Homogeneous	4.88 x 10 ⁻¹²	3.69×10^{-12}	2.58 x 10 ⁻¹²
	Total ^b : Rim	8.35×10^{-12}	6.67×10^{-12}	4.82×10^{-12}

^a The sum of contributions from α (homogeneous) within 4 x 10⁻⁵ m from the surface (Table 3 a), β within 10⁻² m from the surface (Table 3 b) and γ within 0.1 m from the surface.

100 000 y. This clearly shows that for young fuels there is significant impact from β - and γ -radiation while for fuel with an age around 1000 y, H_2O_2 production is completely dictated by α -radiolysis regardless of accessible water volume. For the oldest fuel, where the rate of H_2O_2 production and thereby also the rate of oxidative dissolution is significantly lower, it is interesting to note that the impact of β - and γ -radiation becomes significant as the accessible water volume increases.

The finding that the rim-effect on the dose rate distribution is quite significant is interesting and worth considering in future safety assessments. The dose rate can be up to 3 times higher than predicted from inventories where the rim-effect is not accounted for. However, the effect of a higher dose rate is most probably completely or partially counteracted by a higher content of fission products and heavier actinides in the rim which would reduce the redox reactivity of the UO2-matrix [35]. Previous studies have shown that the presence of dopants in UO2 affects the competition between oxidation by H_2O_2 and surface catalyzed decomposition of H_2O_2 in favour of the latter [36].

As pointed out above, the presence of H₂ in the groundwater efficiently suppress the radiation induced oxidative dissolution of the UO2 matrix. Of the several proposed mechanisms for H2-inhibition of oxidative dissolution of spent nuclear fuel, the most efficient one has been shown to be noble metal catalyzed reduction of oxidized UO2 on the fuel surface [15,37]. The noble metal inclusions (or ε -particles) are composed of fission products that are insoluble in the UO2-matrix and therefore form metallic inclusions. This process can counteract the oxidative dissolution already at quite low H₂-concentrations [15,37]. The content of fission products in spent nuclear fuel is 3-4 % [1]. It is therefore reasonable to assume that the ε -particle surface coverage could be around 1 %. Using the surface coverage and the concentration of dissolved H₂ (calculated from the H₂ pressure and Henry's law) we can calculate the maximum rate of H₂-induced reduction of oxidized UO₂ on the fuel surface [10,13,15]. The resulting maximum rate (corresponding to the maximum inhibiting capacity) for some different H₂-pressures are given in Table 4.

Judging from the results presented in Tables 3 and 4 and the very conservative assumption that the rate of oxidative UO_2 -dissolution corresponds to the maximum dissolution rate (i.e., the rate of H_2O_2 production), we can conclude that radiation induced oxidative dissolution of 15 years old spent nuclear fuel can be completely inhibited at H_2 pressures between 1 and 10 bar. For 1000 years old fuel, 0.1 bar H_2 is sufficient for complete inhibition and for 100 000 years old fuel

 $[^]b$ The sum of contributions from α (rim), β and γ within 4 x 10^{-5} m from the surface.

 $[^]b$ The sum of contributions from α (rim) within 4 x 10^{-5} m from the surface (Table 3 a) and β and γ within 10^{-2} m from the surface.

 $[^]b$ The sum of contributions from α (rim) within 4 x 10^{-5} m from the surface (Table 3 a), β within 10^{-2} m from the surface (Table 3 b) and γ within 0.1 m from the surface.

Table 4 Inhibiting capacity of H₂ at different H₂ pressures.

H ₂ pressure (bar)	Inhibiting capacity (mol $m^{-2} s^{-1}$)
0.1	7.8×10^{-10}
1	7.8×10^{-9}
10	7.8×10^{-8}
40	3.1×10^{-7}

considerably less than 0.1 bar is required. Most probably, radiolytic production of H_2 will be sufficient for the oldest fuel. The impact of radiolytically produced H_2 on radiation-induced oxidative dissolution of UO_2 -based spent nuclear fuel has been explored in more detail in a recent work [37].

4. Conclusions

The SCALE calculations performed in this work give spatial radionuclide distributions in agreement with experimental results obtained using Laser Ablation Inductively Coupled Plasma Mass Spectrometry (LA-ICP-MS). The subsequent MCNP calculations of the dose rate profiles show that the dose rate increases by a factor of 2-3 when accounting for the spatial radionuclide distribution. At the same time, the effect of a higher dose rate is most probably completely or partially counteracted by a higher content of fission products and heavier actinides in the rim which will reduce the redox reactivity of the UO_2 -matrix and thereby favour catalytic decomposition of the dominant radiolytic oxidant, H_2O_2 . In conclusion, it is essential that the spatial radionuclide distribution is accounted for in models describing radiation-induced dissolution of spent nuclear fuel but also in experimental studies focusing on the fuel surface reactivity.

CRediT authorship contribution statement

Karin Andgren: Writing – review & editing, Writing – original draft, Visualization, Methodology, Investigation, Formal analysis, Data curation, Conceptualization. Olivia Roth: Writing – review & editing, Writing – original draft, Project administration, Methodology, Investigation, Formal analysis, Data curation, Conceptualization. Mats Jonsson: Writing – review & editing, Writing – original draft, Methodology, Formal analysis, Data curation, Conceptualization.

Declaration of competing interest

The authors declare the following financial interests/personal relationships which may be considered as potential competing interests: Mats Jonsson reports financial support was provided by Swedish Nuclear Fuel and Waste Management Co. If there are other authors, they declare that they have no known competing financial interests or personal relationships that could have appeared to influence the work reported in this paper.

Acknowledgements

The fuel samples, fabrication and irradiation data were made available by Westinghouse Electric Sweden and OKG Aktiebolag. The LA-ICP-MS study was funded by the European Union's European Atomic Energy Community's (Euratom) Seventh Framework Programme FP7/ 2007–2011 under grant agreement n° 295722 (FIRST-Nuclides project) and performed by Studsvik Nuclear AB.

Svensk Kärnbränslehantering AB is gratefully acknowledged for financial support.

Appendix A. Supplementary data

Supplementary data to this article can be found online at $\frac{\text{https:}}{\text{doi.}}$ org/10.1016/j.net.2025.103814.

References

- R.C. Ewing, Long-term storage of spent nuclear fuel, Nat. Mater. 14 (2015) 252–257.
- [2] A. Martinez-Torrents, D. Serrano-Purroy, R. Sureda, I. Casas, J. de Pablo, Instant release fraction corrosion studies of commercial UO2 BWR spent nuclear fuel, J. Nucl. Mat. 488 (2017) 302–313.
- [3] D.W. Shoesmith, Fuel corrosion processes under waste disposal conditions, J. Nucl. Mater. 282 (2000) 1–31.
- [4] A.S. Kertes, R. Guillaumont, Solubility of UO₂. A comparative review, Nucl. Chem. Waste Manage. 5 (1985) 215–219.
- [5] T. Eriksen, D.W. Shoesmith, M. Jonsson, Radiation induced dissolution of UO₂ based nuclear fuel a critical review of predictive modelling approaches, J. Nucl. Mater. 420 (2012) 409–423.
- [6] A. Barreiro Fidalgo, Y. Kumagai, M. Jonsson, The role of surface-bound hydroxyl radicals in the reaction between H₂O₂ and UO₂, J. Coord. Chem. 71 (2018) 1799–1807.
- [7] E. Ekeroth, O. Roth, M. Jonsson, The relative impact of radiolysis products in radiation induced oxidative dissolution of UO₂, J. Nucl. Mater. 355 (2006) 38–46.
- [8] F. Nielsen, K. Lundahl, M. Jonsson, Simulations of H₂O₂ concentration profiles in the water surrounding spent nuclear fuel, J. Nucl. Mater. 372 (2008) 32–35.
- [9] F. Nielsen, M. Jonsson, Simulations of H₂O₂ concentration profiles in the water surrounding spent nuclear fuel taking mixed radiation fields and bulk reactions into account, J. Nucl. Mater. 374 (2008) 281–285.
- [10] M. Jonsson, F. Nielsen, O. Roth, E. Ekeroth, S. Nilsson, M.M. Hossain, Radiation induced spent nuclear fuel dissolution under deep repository conditions, Environ. Sci. Technol. 41 (2007) 7087–7093.
- [11] N.L. Hansson, M. Jonsson, C. Ekberg, K. Spahiu, Modelling radiation-induced oxidative dissolution of UO2-based spent nuclear fuel on the basis of the hydroxyl radical mediated surface mechanism: exploring the impact of surface reaction mechanism and spatial and temporal resolution, J. Nucl. Mater. 578 (2023) 154369.
- [12] M. Broczkowski, J. Noël, D. Shoesmith, The inhibiting effects of hydrogen on the corrosion of uranium dioxide under nuclear waste disposal conditions, J. Nucl. Mater. 346 (2005) 16–23.
- [13] M. Trummer, S. Nilsson, M. Jonsson, On the effects of fission product noble metal inclusions on the kinetics of radiation induced dissolution of spent nuclear fuel, J. Nucl. Mater. 378 (2008) 55–59.
- [14] M. Trummer, O. Roth, M. Jonsson, H₂ inhibition of radiation induced dissolution of spent nuclear fuel, J. Nucl. Mater. 383 (2009) 226–230.
- [15] M. Trummer, M. Jonsson, Resolving the H₂ effect on radiation induced dissolution of UO₂-based spent nuclear fuel, J. Nucl. Mater. 396 (2010) 163–169.
- [16] F. Nielsen, M. Jonsson, Geometrical α- and β-dose distributions and production rates of radiolysis products in water in contact with spent nuclear fuel, J. Nucl. Mater. 359 (2006) 1–7.
- [17] S. Mougnaud, M. Tribet, S. Rolland, J.-P. Renault, C. Jégou, Determination of alpha dose rate profile at the HLW nuclear glass/water interface, J. Nucl. Mater. 462 (2015) 258–267.
- [18] M. Tribet, S. Mougnaud, C. Jégou, Spent nuclear fuel/water interface behavior: alpha dose rate profile determination for model surfaces and microcracks by using Monte-Carlo methods, J. Nucl. Mater. 488 (2017) 245–251.
- [19] N.L. Hansson, C. Ekberg, K. Spahiu, Alpha dose rate calculations for UO₂ based materials using stopping power models, Nucl. Mater. Energy 22 (2020) 100734.
- [20] A. Siberry, D. Hambley, A.M. Adamska, R. Springell, A geometrical model to describe the alpha dose rates from particulates of UO₂ in water, Rad. Phys. Chem. 188 (2021) 109677.
- [21] A. Siberry, D. Hambley, A.M. Adamska, R. Springell, A mathematical model to describe the alpha dose rate from a $\rm UO_2$ surface, Rad. Phys. Chem. 182 (2021) 109359.
- [22] N.L. Hansson, M. Jonsson, C. Ekberg, K. Spahiu, Geometrical aspects of alpha dose rates from $\rm UO_2$ based fuel, Rad. Phys. Chem. 199 (2022) 110336.
- [23] F. Becker, B. Kienzler, Simulation of alpha dose for predicting radiolytic species at the surface of spent nuclear fuel pellets, Open Chem. 13 (2015) 586–590.
- [24] L.H. Johnson, C. Poinssot, C. Ferry, P. Lovera, Estimates of the Instant Release Fraction of UO₂ and MOX Fuel at T = 0. Nagra NTB 04-08, Nagra, Switzerland, 2004.
- [25] L. Johnson, C. Ferry, C. Poinssot, P. Lovera, Spent fuel radionuclide source-term model for assessing spent fuel performance in geological disposal. Part I: assessment of the instant release fraction, J. Nucl. Mater. 346 (2005) 56–65.
- [26] C. Ferry, J.-P. Piron, A. Poutesquen, C. Poinssot, Radionuclides release from the spent fuel under disposal conditions: re-evaluation of the instant release fraction, in: W.E. Lee, J.W. Roberts, N.C. Hyatt, R.W. Grimes (Eds.), Scientific Basis for Nuclear Waste Management XXXI: Symposium Held in Sheffield, United Kingdom, 16–21 September 2007, Materials Research Society. (Materials Research Society Symposium Proceedings 1107), Warrendale, 2008, pp. 447–454.

- [27] B.T. Rearden, M.A. Jessee (Eds.), SCALE 6.2.3 User Manual, ORNL/TM-2005/39, UT-Battelle, LLC, Oak Ridge National Laboratory, Oak Ridge, TN, 2018.
- [28] C.J. Werner (Ed.), MCNP Users Manual Code Version 6.2, Los Alamos National Laboratory, 2017 report LA-UR-17-29981.
- [29] K.J.E. Zieb, H.G. Hughes, G. Xu, Review of Heavy Charged Particle Transport in MCNP6.2, Los Alamos National Laboratory, 2018 report LA-UR-17-23488.
- [30] M. Berger, J. Coursey, M. Zucker, ESTAR, PSTAR, and ASTAR: computer programs for calculating stopping-power and range tables for electrons, Protons, and Helium Ions (1999). http://physics.nist.gov/Star. (Accessed 1 December 2023).
- [31] A. Puranen, M. Granfors, O. Roth, Laser ablation study of irradiated standard UO₂ fuel and Al/Cr doped UO₂ fuel, in: FIRST Nuclides (D-N°:5.4) − Final (3Rd) Annual Workshop Proceeding "Fast/Instant Release of Safety Relevant Radionuclides from Spent Nuclear Fuel, Bernhard Kienzler, Volker Metz, Lara Duro, Alba Valls, 2014, p. 79.
- [32] M. Granfors, A. Puranen, H.-U. Zwicky, Radial profiling and isotopic inventory analysis of irradiated nuclear fuel using laser ablation ICP-MS", in: Proceedings of Top Fuel 2012, 2012, pp. 191–195, 2nd – 6th September 2012, Manchester, UK.
- [33] B. Pastina, J.A. LaVerne, Effect of molecular hydrogen on hydrogen peroxide in water radiolysis, J. Phys. Chem., A 105 (2001) 9316–9322.
- [34] O. Roth, M. Trummer, M. Jonsson, Factors influencing the rate of radiationinduced dissolution of spent nuclear fuel, Res. Chem. Intermed. 35 (2009) 465–478.
- [35] S. Nilsson, M. Jonsson, H_2O_2 and radiation induced dissolution of UO_2 and SIMFUEL pellets, J. Nucl. Mater. 410 (2011) 89–93.
- [36] R. Pehrman, M. Trummer, C.M. Lousada, M. Jonsson, On the redox reactivity of doped UO₂ pellets – influence of dopants on the H₂O₂ decomposition mechanism, J. Nucl. Mater. 430 (2012) 6–11.
- [37] N.L. Hansson, M. Jonsson, Exploring H₂-effects on radiation-induced oxidative dissolution of UO₂-based spent nuclear fuel using numerical simulations, Rad. Phys. Chem. 210 (2023) 111055.